EPJ Web of Conferences **202**, 06005 (2019) https://doi.org/10.1051/epjconf/201920206005
CHARM 2018

The inclusive reconstruction of Charmed Mesons on B-factory

Olga Gzhymkovska[1,*] (on behalf of the Belle Collaboration)

[1]Institute of Nuclear Physics PAS,
Radzikowskiego Str., 152, Krakow, POLAND

Abstract. We present the study of the inclusive branching ratios of the double charmed decays with strangeness $B \to \bar{D}^{(*)} D^{(*)}_{s(J)}$. The study based on the missing mass distributions in inclusive transitions $B \to \bar{D}^{(*)} X$, and thus in a way free from the assumptions about resonance decays $D^{(*)}_{s(J)}$. There are also presented the perspective of such studies on the next generation Belle II experiment.

1 Introduction

The main subject of this study are double-charmed (quasi)two-body decays of beautiful mesons $B \to \bar{D}^{(*)} D^{(*)}_{s(J)}$. At the quark level this is a process dominated by the transition $b \to W^- c \to c\bar{c}s$, and its diagrams are shown in fig. 1. In the context of the standard model such transitions occur as a result of the weak interaction through the exchange of charged intermediate bosons $W^{\pm}$. The coupling constants in the vertices, and thus the amplitudes of the processes, are modified by the appropriate factor resulting from the CKM matrix.

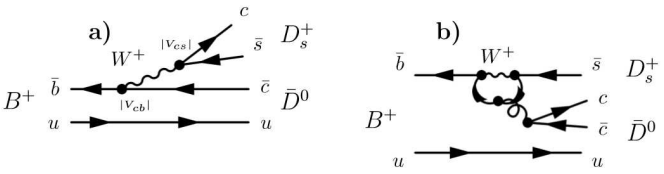

Figure 1. Quark diagrams of the process $B^+ \to \bar{D}^{0(*)} D^{(*)}_{s(J)}$.

In the CKM mechanism, the most favored are the transitions between quarks of the same generation, despite this transition $b \to c$ (fig. 1a) will be dominating in the B decays, since the $b \to t$ process is not allowed kinematically because of the very large mass of the t quark. The transition $c \to s$ is preferred as a transition within the same family of quarks. It follows from the above considerations that the $B \to \bar{D}^{(*)} D^{(*)}_{s(J)}$ decays will be relatively frequent [1]. The branching ratios of these decays depend, however, on the properties of the $D_{s(J)}$ mesons produced in the final state, which is discussed in the following chapters. In addition to the

*e-mail: olga.grzymkowska@ifj.edu.pl

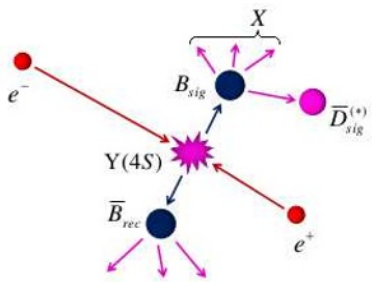

Figure 2. Diagram of the studied events.

dominant tree-type diagram (fig. 1a), the tested decays may also take place via a higher order penguin diagram (fig. 1b), where in the loop, in addition to the $W^{\pm}$ boson there is also an exchange of quarks u, c, t. However, the contribution of these amplitudes to SM is negligible.

2 General scheme of the analysis

One of the biggest advantages of B factories compared to hadronic accelerators (Tevatron or LHC) is the thorough knowledge of the initial state and production process of B mesons. This property can be used to reconstruct one of the B mesons, so-called B tagging, denoted as B_{tag}. Full or partial B_{tag} reconstruction provides information about the momentum and quantum numbers of the second B meson produced in a given event, so-called signal B that will be denoted as B_{sig}. As part of this work a full reconstruction of B_{tag} in purely hadron final states was used. In the next step the charmed meson $D^{(*)}_{\text{sig}}$ coming from the B_{sig} decay is exclusively reconstructed. The above procedure contributes simultaneously to the combinatorial background from other $B\bar{B}$ decays and continuum events suppression.

The mass M_X of the remaining unreconstructed meson decay products B_{sig}, denoted as X, is calculated as the missing mass:

$$M_X = \sqrt{p^2_{\text{miss}}} = \sqrt{(p(\Upsilon(4S)) - p(B_{\text{tag}}) - D^{(*)}_{\text{sig}})^2}, \tag{1}$$

where p is a four-momentum of the particle. The $D^{(*)}_{s(J)}$ mesons from two-body decays $B \to \bar{D}^{(*)} D^{(*)}_{s(J)}$ will appear as reinforcements in the M_X distribution at values corresponding to their mass. Multi-body decays of the $B \to \bar{D}^{(*)} n\pi m K$ type (n and/or $m > 1$) will be in M_X visible as broad structures and in this analysis will be treated as a background.

2.1 $\bar{D}^{(*)}_{\text{sig}}$ meson reconstruction

$\bar{D}^{(*)}_{\text{sig}}$ mesons are reconstructed in decay channels given below:

- $\bar{D}^0 \to K^+\pi^-, \bar{D}^0 \to K^+\pi^-\pi^-\pi^+, \bar{D}^0 \to K^+\pi^-\pi^0$
- $D^- \to K^+\pi^-\pi^-, D^- \to K^0_S\pi^-$
- $D^{*-} \to \bar{D}^0\pi^-, D^{*-} \to D^-\pi^0$
- $\bar{D}^{*0} \to \bar{D}^0\pi^0$

3 Reference channels

The analysis is covering the missing mass range $1.7 < M_X < 2.7$ GeV, which contains the majority of resonances in the $c\bar{s}$ system. The upper M_X mass area has been excluded from the analysis due to the low $\bar{D}^{(*)}_{\mathrm{sig}}$ reconstruction efficiency. Missing mass range $1.7 < M_X < 2.2$ GeV was treated as a control. Signal quantities and branching ratios for individual channels are determined from the fit of the missing mass distributions in the tested M_X range, simultaneously for all decay channels. All fits are made using the maximum likelihood method event after event. The analysis is carried out in a mode called "user blind", i.e. all signal measurement elements are determined from the Monte Carlo samples and control areas in the data.

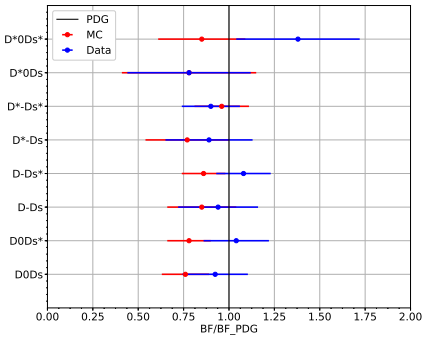

Figure 3. Branching ratios for reference channels for GMC (red) and data (blue) relatively to PDG values [2].

4 Signal measurement

$B^+ \to \bar{D}^{(*)} D^{(*)}_{s(J)}$ decays signals has been extracted by the fitting of the missing mass distribution. To determine the number of signal events and its shape parameters, the unbinned extended maximum likelihood fit for the M_X variable including crossfeeds between individual decay channels was used. Probability density functions (PDF) for PDF_{S_i} signals were parameterized using the Gauss function:

$$PDF_{S_i} = \frac{1}{\sigma_i \sqrt{2\pi}} \exp\left(-\frac{(M_{X_i} - \mu_i)^2}{2\sigma_i^2}\right) \tag{2}$$

(index i numbers signal channels), while for background PDF^i_{bkg} are represented by normalized Chebychev polynomials, 1st, 2nd or 3rd order:

$$PDF^i_{bkg} = Cheb^i_{1,2,3}(M_{X_i}) \tag{3}$$

Probability density functions for crossfeeds $PDF^{i\to k}_{x-feed}$ are described using normalized histograms:

$$PDF^{i\to k}_{x-feed} = f^i_{x-feed}(M_{X_k}), \tag{4}$$

received from the GMC samples. The probability function has the following form:

$$\mathcal{L} = \frac{(N_{sig} + N_{bkg})^N \cdot e^{(N_{sig}+N_{bkg})}}{N} \prod_{j=1}^{N} (\sum_i (N_{sig}^{i\to i}(\mathcal{B}_i) \cdot PDF_{S_i}(M_{X_i}^j) + N_{bkg}^i \cdot PDF_{bkg}^i(M_{X_i}^j) + \sum_k N_{sig}^{i\to k}(\mathcal{B}_i) \cdot PDF_{x-feed}^{i\to k}(M_{X_k}^j))), \quad (5)$$

where N is the total number of fitted events, $N_{\rm sig}$ and $N_{\rm bkg}$ are the corresponding total numbers of signal and background events, $M_{X_l}^j$ denotes missing mass of j-th event calculated for l channel, $N_{\rm sig}^{i\to k}(\mathcal{B}_i)$ and $N_{\rm sig}^{i\to i}(\mathcal{B}_i)$ are defined by the formulas:
$N_{\rm sig}^{i\to k}(\mathcal{B}_i) = N_{B\bar{B}} \cdot \mathcal{B}_i \cdot \varepsilon_{i\to k}^{x-feed}, (i \neq k)$,
$N_{\rm sig}^{i\to i}(\mathcal{B}_i) = N_{B\bar{B}} \cdot \mathcal{B}_i \cdot \varepsilon_{i\to i}$ and depend on the measured branching ratios $\mathcal{B}_i$, which are the free fit parameters. In addition, the free parameters are the numbers of background events $N_{\rm bkg}^i$. The adjustment was carried out at fixed ε_i and μ_i values determined from the dedicated SMC samples.

4.1 Results for GMC in the entire M_X range

The results of *PDF* fitting (eq. 5) to the missing mass distribution in the entire test range obtained for GMC are shown in fig. 4. In addition to the signals from reference channels $B^+ \to \bar{D}^{(*)} D_{s(J)}^{(*)}$ are visible the structures from higher excited $c\bar{s}$ states: $D_{s0}^*(2317)$ and $D_{s1}(2460)$, which are included in the general MC. For $\bar{D}_{\rm sig} = \bar{D}^0, \bar{D}^{*0}$ the observed background is quite high in the reference area and grows strongly with an increase of M_X. This increase is exponential. The dominant background component for $B^+ \to \bar{D}^{(*)0} D_{s(J)}^{(*)}$ decays is the background from B^+B^- pairs.

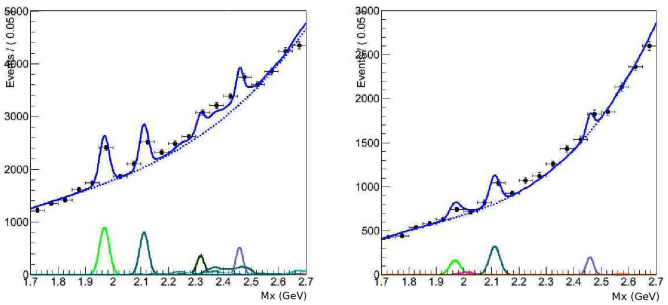

Figure 4. GMC fit results to the full range missing mass distribution for $B^+ \to \bar{D}^0 D_{s(J)}^{(*)}$ (left) and for $B^+ \to \bar{D}^{*0} D_{s(J)}^{(*)}$ (right). For both figures, the Gauss curves correspond to resonances of D_s (light green), D^* (pink), D_s^* (dark green), $D_{s1}(2460)$ (purple); on the (a) graph an irregular structure describes crossfeeds from channels $B^+ \to \bar{D}^{*0} D_{s(J)}^{(*)}$ and $B^0 \to D^{*-} D_{s(J)}^{(*)}$.

5 Numerical results for MC in the M_X range 1.7 - 2.7 GeV

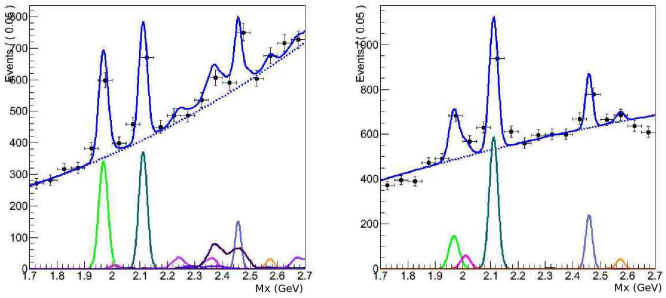

Figure 5. GMC fit results to the full range missing mass distribution for $B^0 \to \bar{D}^- D^{(*)}_{s(J)}$ (left) and for $B^0 \to \bar{D}^{*-} D^{(*)}_{s(J)}$ (right). The description of the resonances is given on the previous figure (fig. 4).

Decay channel	$\mathcal{B}$ Data (%)	$\mathcal{B}$ PDG (%)	Inclusive study (%) [3]	Theory (%) [4]
$B^+ \to \bar{D}^0 D_s$	$0.83 \pm 0.08 \pm 0.09 \pm 0.04$	0.90 ± 0.09	$1.33 \pm 0.18 \pm 0.32$	$1.00^{+0.13}_{-0.28}$
$B^+ \to \bar{D}^0 D^*_s$	$0.79 \pm 0.08 \pm 0.09 \pm 0.04$	0.76 ± 0.16	$0.93 \pm 0.18 \pm 0.19$	$0.84^{+0.23}_{-0.31}$
$B^+ \to \bar{D}^{*0} D_s$	$0.64 \pm 0.15 \pm 0.06 \pm 0.05$	0.82 ± 0.17	$1.21 \pm 0.23 \pm 0.20$	$1.03^{+0.13}_{-0.32}$
$B^+ \to \bar{D}^{*0} D^*_s$	$2.36 \pm 0.26 \pm 0.24 \pm 0.18$	1.71 ± 0.24	$1.70 \pm 0.26 \pm 0.24$	$2.80^{+0.40}_{-0.90}$
$B^0 \to D^- D_s$	$0.68 \pm 0.08 \pm 0.07 \pm 0.03$	0.72 ± 0.08	$0.90 \pm 0.18 \pm 0.14$	$0.93^{+0.12}_{-0.26}$
$B^0 \to D^- D^*_s$	$0.80 \pm 0.09 \pm 0.08 \pm 0.04$	0.74 ± 0.02	$0.67 \pm 0.20 \pm 0.11$	$0.78^{+0.21}_{-0.29}$
$B^0 \to D^{*-} D_s$	$0.71 \pm 0.10 \pm 0.08 \pm 0.02$	0.80 ± 0.11	$0.57 \pm 0.16 \pm 0.09$	$0.95^{+0.13}_{-0.29}$
$B^0 \to D^{*-} D^*_s$	$1.59 \pm 0.15 \pm 0.17 \pm 0.05$	1.77 ± 0.14	$1.65 \pm 0.23 \pm 0.19$	$2.60^{+0.30}_{-0.80}$
	$\pm\Delta_{expected}(\%)$			
$B^+ \to \bar{D}^0 D_{s1}(2460)$	$\pm 0.051 \pm 0.018 \pm 0.08$	$0.31^{+0.1}_{-0.09}$	$0.43 \pm 0.16 \pm 0.13$	$0.44^{+0.16}_{-0.19}$
$B^+ \to \bar{D}^{*0} D_{s1}(2460)$	$\pm 0.17 \pm 0.09 \pm 0.07$	1.2 ± 0.3	$1.12 \pm 0.26 \pm 0.20$	$2.10^{+0.30}_{-0.80}$
$B^0 \to D^- D_{s1}(2460)$	$\pm 0.05 \pm 0.02 \pm 0.01$	0.35 ± 0.11	$0.26 \pm 0.15 \pm 0.07$	$0.40^{+0.16}_{-0.17}$
$B^0 \to D^{*-} D_{s1}(2460)$	$\pm 0.09 \pm 0.06 \pm 0.02$	0.93 ± 0.22	$0.88 \pm 0.20 \pm 0.14$	$1.90^{+0.40}_{-0.70}$

Table 1. Comparison of the measured branching ratios with the PDG values [2], inclusive measurements of the BaBar experiment [3] and theoretical predictions [4]. The uncertainties quoted are due to statistics (first), experimental systematic (second) errors and uncertainties of branching fractions for the decays of intermediate resonances for a given channel (third).

6 Summary

On Belle data we can improve the BF measurements by reducing statistical and systematic uncertainties by factor 3 in respect to the current measurements.

On Belle II data (50 times more) we can study the properties of higher excited states of $D^{(*)}_{s(J)}$ mesons. Further improvement can come from the including in the simultaneous fit D^{**} mesons.

With the similar method we can study recoil mass in respect to D_s hence reconstruct inclusively $D^{(**)}$ mesons.

References

[1] Y. Amhis *et* al. [HFLAV Collaboration], Eur. Phys. J. C **77** (2017) no.12, 895 doi:10.1140/epjc/s10052-017-5058-4 [arXiv:1612.07233 [hep-ex]].

[2] K. A. Olive *et* al. [Particle Data Group], Chin. Phys. C **38** 090001 (2014). doi:10.1088/1674-1137/38/9/090001

[3] B. Aubert *et al.*, [BaBar Collaboration] Phys. Rev. D74:031103 (2006).
[4] Fu Hui-feng, Wang Guo-Li *et al.*, Chin. Phys. Lett. Vol. 28, No. 12 121301, (2011), arXiv:1202.1221v1.